

Modelling machine tool dynamics using a distributed parameter tool–holder joint interface

Keivan Ahmadi, Hamid Ahmadian*

School of Mechanical Engineering, Iran University of Science and Technology, Narmak, Tehran 16844, Iran

Received 7 October 2006; received in revised form 5 March 2007; accepted 13 March 2007

Available online 19 March 2007

Abstract

Increasing productivity in machining process demands high material removal rate in stable cutting conditions and depends strongly on dynamic properties of machine tool structure. Combined analytical–experimental procedures based on receptance coupling substructure analysis (RCSA) are employed to determine the stability of machine operating conditions at different tool configurations. The RCSA employs holder–spindle experimental mobility measurements in conjunction with an analytical model for the tool to predict the dynamics of different sets of tool and holder–spindle combinations without the need for repeated mobility measurements. In this paper an alternative approach using the concept of tool on resilient support is adopted to predict the machine tool dynamics in various tool configurations. In the proposed model the tool, represented by an analytical model, is partly resting on a resilient support provided by the holder–spindle assembly. The support dynamic flexibility is measured by performing vibration tests on the holder–spindle assembly. Tool–holder joint interface characteristics are included in the model by considering a distributed elastic interface layer between the holder–spindle and the tool shank part. The distributed interface layer takes into account the change in normal contact pressure along the joint interface and comparing with the lumped joint model used in RCSA it allows more detailed representation of the joint interface flexibility and damping which have crucial roles in machine dynamics. Experiments are conducted to demonstrate the efficiency of proposed model in prediction of milling operation dynamics and it is shown that the model is capable of accurately predicting the dynamic absorber effect of spindle in a tool tuning practice.

© 2007 Elsevier Ltd. All rights reserved.

Keywords: Chatter vibration; Machining dynamics; Stability lobes; Tool tuning

1. Introduction

Machine tool regenerative chatter is the main obstacle in high-speed machining [1]; it produces unstable vibration of tool due to the feedback between subsequent cuts, and leads to unwanted effects such as poor dimensional accuracy and tool or work piece damage. Regenerative chatter suppression is mainly performed by choosing proper depth of cut in each cutting speed. Knowledge of machine tool frequency responses is a primary requirement in determining the stable cutting conditions. Frequency responses of machine tool structure, commonly obtained by experimental mobility measurements, have been used by many researchers to determine the stable cutting condition

[2–7]. The process of stability analysis becomes expensive and time consuming when experimental measurements are needed for each individual combination of spindle–holder and tool configurations. This creates a demand for predictive models that are capable of determining the dynamics of different tool/spindle/holder configurations without the need for vibration measurement repetitions. For slender tools where the system dynamics is mostly dominated by the tool modes, flexible tool and rigid holder models are commonly used [8–11]. For tools with considerable lateral stiffness the dynamics of machining process is strongly dependent on spindle behavior. Schmitz et al. [12,13] treated the tool–holder–spindle assembly as two separate substructures, i.e. the tool and the holder–spindle, and employed receptance coupling substructure analysis (RCSA) to predict the tool tip frequency responses. They predicted tool frequency responses by

*Corresponding author. Tel.: +98 21 73912907; fax: +98 21 77240488.
E-mail address: ahmadian@iust.ac.ir (H. Ahmadian).

combining the experimentally measured holder–spindle frequency responses and the frequency responses of the tool which are obtained from an analytical model. Employing RCSA enables one to predict the changes in the tool tip frequency responses due to any variation in the tool configuration, and removes the need for repeated frequency response measurements in practices such as tool tuning.

The RCSA requires the response of the substructures at all degrees of freedom of the joint interface. Direct measurement of moments and rotational deformations at the joint interface is impractical. Due to the difficulties involved in measurement of rotational motions and moments, Schmitz et al. [12,13] considered only translational motion of the spindle substructure. In practice tool bends at the holder joint interface and ignoring the rotational flexibilities in modelling produces inaccurate predictions of machine dynamics. Park et al. [14] proposed algorithms for determination of rotational responses of tool/holder joint interface using two adjacent translational vibration experiments. Movahhedy et al. [15] proposed an equivalent lumped joint model between the tool and holder replacing the common translational–rotational spring sets by two parallel linear springs, avoiding rotational receptance measurements in RCSA. Duncan and Schmitz [16] used RCSA to predict the dynamics of tool/holder/spindle assembly and included the rotational flexibility of spindle assuming that each spindle mode at the joint interface can be approximated locally using an equivalent clamped–free Euler–Bernoulli beam. They identified the modal parameters of spindle and based on the obtained information geometrical specifications of the equivalent beam with similar modal properties are used to predict the rotational dynamics of the support. Later Schmitz et al. [17–19] employed the concept of multi-point coupling to provide more accurate models of the joint interfaces stiffness and damping. More recently, Erturk et al. [20,21] proposed an analytical method that uses Timoshenko beam theory to calculate the tool point response in a given combination by using RCSA. They used the model in examining the effects of individual bearing and contact parameters on tool tip response and the effects of spindle, holder and tool parameters on chatter stability.

In this paper the tool dynamics is modelled considering the tool inserted shank is resting on a resilient support. The support, provided by the spindle–holder, is represented by a damped-elastic foundation capable of simulating the dominant translational and rotational deformations of spindle in each individual frequency. The support receptance functions are measured using a set of mobility experiments on spindle–holder assembly and are directly employed in the analytical solution to encounter dynamic properties of the support. The joint interface between the tool and the holder is modelled using an elastic interface layer. Introduction of this layer enables one to take into account the variation in contact stiffness due to tool changes, interface contact pressure distribution, etc. The

interface stiffness is assumed to be a complex valued function to include the joint interface damping effects. The interface stiffness can be defined as a function along the tool inserted shank length. This enables the analyst to introduce the contact stiffness in more detail taking into account variations of normal pressure between the tool and holder. The stiffness and damping parameters of the tool–holder joint interface represented using a distributed elastic layer is identified by performing an impact test on the tool–holder–spindle assembly. These parameters are identified by minimizing the difference between the measured and calculated receptance curves of the assembly. An analytical solution is developed for dynamic response of the assembly and using the obtained solution its dynamic behavior and stability are investigated in different machining conditions.

The remaining of the paper runs as follows. In Section 2 the proposed model consisting of a tool partly resting on a flexible support is introduced and its frequency response at the tool tip is determined using an analytical approach. Experimental procedures are conducted in Section 3; holder–spindle frequency responses are measured using impact hammer test and are used to calculate the support dynamic stiffness. Also in this section the tool–holder interface characteristics are identified by comparison of measured and calculated receptance curves at the tool tip. In Section 4 the presented model is used to predict the milling dynamics and to find the optimum tool length for a stable cutting condition. A tool tuning practice is performed using the presented model and its predictions are validated by experimentally measured responses. Finally, some conclusions are made in Section 5.

2. Model development

In development of a dynamic model for machining operations, tool is modelled using continuous beam theory partly resting on a resilient support; the support resembles spindle/holder dynamic effects. In this model, shown in Fig. 1, tool is represented using a step beam with two sections, namely inserted shank part and the overhung portion. A tool with more complicated geometry can be represented using a beam model with variable cross-sections or a finite element model. The joint interface between the inserted shank portion of the tool and the holder is represented by a zero thickness elastic layer. The dynamics of the tool inserted shank part is considered as an Euler–Bernoulli beam resting on an elastic support and is defined using the following governing equation:

$$EI_1 \frac{\partial^4 U_1(x, t)}{\partial x^4} + m_1 \frac{\partial^2 U_1(x, t)}{\partial t^2} = K(x)[v(x, t) - U_1(x, t)],$$

$$0 \leq x \leq L_1, \quad (1)$$

where $U_1(x, t)$ is lateral displacement of the tool inserted shank, $v(x, t)$ is the lateral displacement of the tool–holder, E is Young modulus of the tool material, L_1 , I_1 , m_1 are,

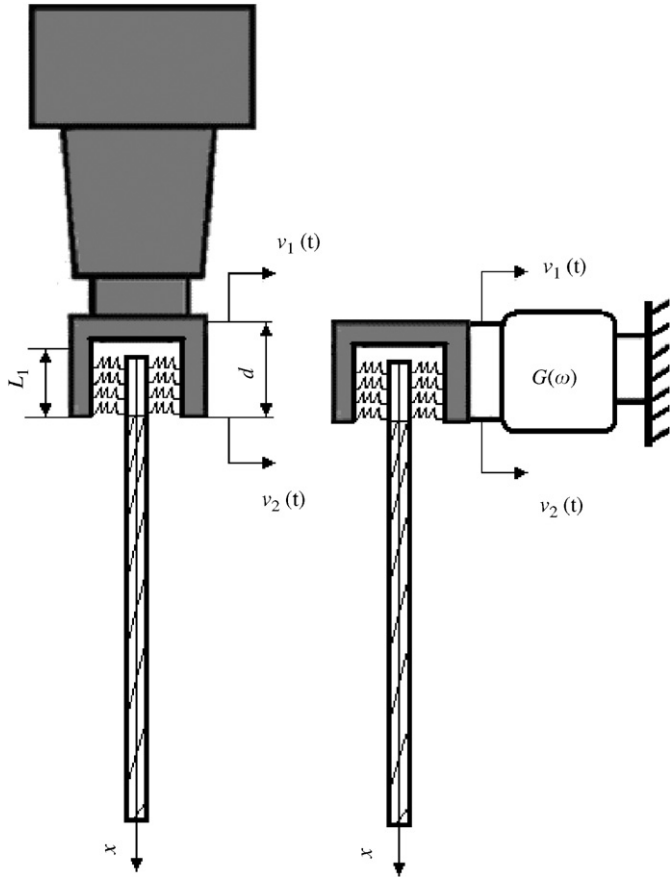


Fig. 1. Schematic view of tool-holder-spindle assembly and its representative model.

respectively, the length, second moment of inertia and mass per unit length of the tool inserted shank and $K(x)$ is the elastic interface layer stiffness coefficient. Stiffness of the layer is assumed to vary along the tool-holder joint interface. The elastic layer stiffness coefficient is a function of normal pressure between holder and the tool inserted shank, the contact surfaces material, the surface finish, etc. It is assumed that there is no slip between these two parts during machining operations and stiffness coefficient remains constant. Schmitz et al. [18,19] and Hanna et al. [22] have obtained typical functions for the normal pressure distribution between tool, holder and spindle through numerical simulations. The stiffness of elastic interface layer is proportional to the normal pressure, therefore a parametric stiffness distribution based on the joint type (shrink fit, etc.) is selected and the stiffness parameters can be identified by matching experimentally recorded responses. These coefficients are assumed to be complex valued to include a displacement-dependent energy dissipation mechanism in the joint interface i.e.:

$$K(x) = k(x)(1 + i\eta), \quad (2)$$

where $k(x)$ and η are the joint interface stiffness and its structural damping factor. The selected damping mechanism is consistent with physics involved in the joint and produces a more representative model of damping

compared to the viscous damping model commonly adopted in other machine tool dynamic models.

The dynamics of overhung portion of the tool is also defined using Euler-Bernoulli beam theory as

$$EI_2 \frac{\partial^4 U_2(x, t)}{\partial x^4} + m_2 \frac{\partial^2 U_2(x, t)}{\partial t^2} = 0, \quad L_1 \leq x \leq L, \quad (3)$$

where $U_2(x, t)$ is lateral displacement of the tool overhung portion, and $L - L_1, I_2, m_2$ are the length, second moment of inertia and mass per unit length of overhung portions of the tool. The proposed model described in Eqs. (1) and (3) determines the tool dynamics under different configurations and loadings.

In tool dynamic analysis one requires the tool tip frequency response function. This function can be obtained by calculating the tip response to a unit harmonic excitation applied at the same location. The boundary conditions at the tool tip in the presence of unit harmonic excitation are unit harmonic shear force and zero moment; this is expressed as

$$-EI_2 \frac{\partial^3 U_2(L, t)}{\partial x^3} = e^{i\omega t}, \quad (4a)$$

$$\frac{\partial^2 U_2(L, t)}{\partial x^2} = 0. \quad (4b)$$

The boundary conditions on the other end of the tool are zero shear force and moment, i.e.:

$$\frac{\partial^2 U_1(0, t)}{\partial x^2} = 0, \quad (4c)$$

$$\frac{\partial^3 U_1(0, t)}{\partial x^3} = 0. \quad (4d)$$

The tool is modelled using a step beam with two sections. The compatibility requirements for the solutions of these two parts at the interface are continuity of displacements, slopes, moments and shear forces. These requirements set the following conditions:

$$U_1(L_1, t) - U_2(L_1, t) = 0, \quad (5a)$$

$$\frac{\partial U_1(L_1, t)}{\partial x} - \frac{\partial U_2(L_1, t)}{\partial x} = 0, \quad (5b)$$

$$EI_1 \frac{\partial^2 U_1(L_1, t)}{\partial x^2} - EI_2 \frac{\partial^2 U_2(L_1, t)}{\partial x^2} = 0, \quad (5c)$$

$$EI_1 \frac{\partial^3 U_1(L_1, t)}{\partial x^3} - EI_2 \frac{\partial^3 U_2(L_1, t)}{\partial x^3} = 0. \quad (5d)$$

Steady-state solutions for the described linear system expressed using the partial differential Eqs. (1), (3) are of the following form:

$$U_1(x, t) = \Phi(x)e^{i\omega t}, \quad (6)$$

$$U_2(x, t) = \Psi(x)e^{i\omega t}, \quad (7)$$

where the tool deformed shapes $\Phi(x)$ and $\Psi(x)$ are complex valued functions due to non-proportional damping nature of the system. These deformed shapes are obtained by satisfying the boundary conditions (4) and compatibility requirements (5).

The holder–spindle assembly motion in the inserted shank region $v(x, t)$ acts as a forcing function in governing Equation (1) and under unit harmonic excitation it can be expressed using translational displacements of two neighboring points on the tool support with the distant d , shown in Fig. 1, as

$$v(x, t) = \left[v_2 + \left(\frac{L_1 - x}{d} \right) (v_1 - v_2) \right] e^{i\omega t}, \quad 0 < x < L_1, \quad (8)$$

where v_1 and v_2 are the deformation amplitudes at points 1 and 2 on the tool support due to single harmonic excitations at tool tip. The complex frequency-dependent deformation amplitudes v_1 and v_2 are in fact cross-frequency responses between these points and the tool tip. Alternatively, one may express deformations v_1 and v_2 in terms of effective forces applied to points 1 and 2 from tool inserted shank:

$$\begin{Bmatrix} v_1 \\ v_2 \end{Bmatrix} = [G] \begin{Bmatrix} f_1 \\ f_2 \end{Bmatrix}. \quad (9)$$

In the above force-displacement relations the 2×2 symmetric frequency-dependent matrix $[G]$ contains $G_{ij}(\omega)$, $i, j = 1, 2$, the measured direct and cross-frequency response functions at points 1 and 2, and f_1, f_2 are the effective applied forces on the holder due to movement of tool shank part. The distributed force applied on the holder $K(x)(\Phi(x) - v(x))$ is replaced by the concentrated forces f_i , $i = 1, 2$, that produce equivalent shear and bending effects on the holder–spindle assembly:

$$f_2 = \int_0^{L_1} \left(1 - \frac{L_1 - x}{d} \right) K(x)(\Phi(x) - v(x)) dx,$$

$$f_1 = \int_0^{L_1} \left(\frac{L_1 - x}{d} \right) K(x)(\Phi(x) - v(x)) dx. \quad (10)$$

An explicit relationship between v_1, v_2 and tool inserted shank part motion $\Phi(x)$ is defined using Eqs. (9)–(10) that is:

$$\begin{Bmatrix} v_1 \\ v_2 \end{Bmatrix} = (I_{2 \times 2} + [G][J])^{-1} [G] \begin{Bmatrix} \int_0^{L_1} \left(\frac{L_1 - x}{d} \right) K(x)\Phi(x) dx \\ \int_0^{L_1} \left(1 - \frac{L_1 - x}{d} \right) K(x)\Phi(x) dx \end{Bmatrix}, \quad (11)$$

where

$$[J] = \int_0^{L_1} K(x) \begin{bmatrix} \left(\frac{L_1 - x}{d} \right)^2 & \left(1 - \frac{L_1 - x}{d} \right) \left(\frac{L_1 - x}{d} \right) \\ \left(1 - \frac{L_1 - x}{d} \right) \left(\frac{L_1 - x}{d} \right) & \left(1 - \frac{L_1 - x}{d} \right)^2 \end{bmatrix} dx. \quad (12)$$

$$a_n = \frac{\left(-\frac{K_{n-6}}{d} + \frac{K_{n-5}L_1}{d} \right) v_1 + \left(\frac{K_{n-6}}{d} + K_{n-5} \left(1 - \frac{L_1}{d} \right) \right) v_2 - (k_0 - m_1\omega^2) a_{n-4} - \sum_{j=1}^{n-5} K_j a_{n-4-j}}{(n-1)(n-2)(n-3)(n-4)EI_1}, \quad n > 6. \quad (16)$$

Employing the frequency responses obtained from measurement directly into the analysis introduces the true nature of mass, stiffness and damping effects of the

holder–spindle assembly. Having obtained the holder motion due to tool tip excitation, we may solve Eq. (1) and obtain the response of tool inserted shank part.

Response of the tool inserted shank modelled as a beam on elastic foundation with variable support stiffness is expressed using a power series [23]. One may introduce the interface layer stiffness function in a polynomial form:

$$K(x) = \sum_{p=0}^P K_p x^p. \quad (13)$$

Such a polynomial can be viewed as Taylor series expansion of the actual interface stiffness function. Correspondingly, the deformed shape for the tool inserted shank is assumed in the following power series format:

$$\Phi(x) = \sum_{n=1}^N a_n x^{n-1}, \quad (14)$$

where $N - 1$ is the power series order, defined by the analyst, depending on the desired accuracy, and a_n , $n = 1, 2, \dots, N$, are complex coefficients. As will be shown only four of these coefficients are independent and the rest of the coefficients are expressed as a function of these four independent parameters. Relations between the coefficients of inserted shank part of the tool solution are obtained by substituting the power series solution into the governing equation (1). This leads to the following relations:

$$EI_1 \sum_{n=1}^N (n-1)(n-2)(n-3)(n-4) a_n x^{n-5} + \left(\sum_{p=0}^P K_p x^p - m\omega^2 \right) \sum_{n=1}^N a_n x^{n-1} = K(x) \left[v_2 + (v_2 - v_1) \left(\frac{x - L_1}{d} \right) \right]. \quad (15)$$

Eq. (15) must be true for all values of x ; this leads to the following recursive relations:

$$a_5 = \frac{1}{24EI_1} \left[\left(\frac{K_0 L_1}{d} \right) v_1 + \left(K_0 \left(1 - \frac{L_1}{d} \right) \right) v_2 - (K_0 - m_1\omega^2) a_1 \right],$$

$$a_6 = \frac{1}{120EI_1} \left[\left(\frac{K_1 L_1}{d} - \frac{K_0}{d} \right) v_1 + \left(\frac{K_0}{d} + K_1 \left(1 - \frac{L_1}{d} \right) \right) v_2 - (K_0 - m_1\omega^2) a_2 - K_1 a_1 \right],$$

The polynomial coefficients, a_n , $5 \leq n \leq N$, are linearly dependent on a_1, a_2, a_3, a_4, v_1 and v_2 through recursive relations (16). These recursive relations can be written in

matrix notation as

$$\begin{Bmatrix} a_1 \\ a_2 \\ \vdots \\ a_N \end{Bmatrix} = [T_v]_{N \times 2} \begin{Bmatrix} v_1 \\ v_2 \end{Bmatrix} + [T_a]_{N \times 4} \begin{Bmatrix} a_1 \\ a_2 \\ a_3 \\ a_4 \end{Bmatrix}. \quad (17)$$

Eq. (11) can be further simplified and a direct relation between v_1 , v_2 and coefficients a_n , $n = 1, \dots, N$, is obtained as

$$\begin{Bmatrix} v_1 \\ v_2 \end{Bmatrix} = (I_{2 \times 2} + [G][J])^{-1} [G][R] \begin{Bmatrix} a_1 \\ a_2 \\ \vdots \\ a_N \end{Bmatrix}. \quad (18)$$

Components of matrices $[T_v]$, $[T_a]$ and $[R]$ are derived in Appendix A and I is an identity matrix. Eqs. (17) and (18) form a set of matrix equations from which the coefficients of the assumed polynomial a_n , $1 \leq n \leq N$, can be obtained as follows:

$$\begin{Bmatrix} a_1 \\ a_2 \\ \vdots \\ a_N \end{Bmatrix} = [S]_{N \times 4} \begin{Bmatrix} a_1 \\ a_2 \\ a_3 \\ a_4 \end{Bmatrix},$$

$$[S] = (I_{N \times N} - [T_v](I_{2 \times 2} + [G][J])^{-1} [G][R])^{-1} [T_a]. \quad (19)$$

Having obtained a parametric solution for the tool inserted shank part in terms of a_n , $n = 1, \dots, 4$, we turn our attention to the solution for the overhung part of the tool.

Deformed shape of the tool overhung portion can be obtained by substituting the solution form defined in Eq. (7) into the governing equation for this portion of the tool expressed in Eq. (3). This results in the following ordinary differential equation in terms of the function $\Psi(x)$:

$$\Psi^{IV}(x) - \lambda^4 \Psi(x) = 0, \quad \lambda^4 = \frac{m_2 \omega^2}{EI_2}. \quad (20)$$

Solution to the above ordinary differential equation is of the following form with the complex coefficients C_i , $i = 1, \dots, 4$:

$$\Psi(x) = C_1 e^{i\lambda x} + C_2 e^{-i\lambda x} + C_3 e^{\lambda x} + C_4 e^{-\lambda x}, \quad L_1 \leq x \leq L. \quad (21)$$

There are eight independent complex valued coefficients namely C_i , a_i , $i = 1, \dots, 4$, which need to be specified in order to determine the tool response. They are specified by satisfying the boundary conditions (4) and the compatibility requirements (5). The given boundary conditions and compatibility requirements form a set of eight linear equations in terms of these eight independent coefficients

and in general may be written in the following form:

$$[Z(\omega)] \begin{Bmatrix} C_1 \\ \vdots \\ C_4 \\ a_1 \\ \vdots \\ a_4 \end{Bmatrix} = \begin{Bmatrix} 1 \\ 0 \\ \vdots \\ \vdots \\ \vdots \\ 0 \end{Bmatrix}, \quad (22)$$

where $[Z(\omega)]$ is a full rank square matrix (its entries are given in Appendix A) and entries of right-hand side vector are all zero except for the first entry which is one, due to the fact that only Eq. (4a) is non-homogenous and the rest of boundary conditions (4b)–(4d) and compatibility requirements (5) are homogenous. The unknown coefficients vector can be determined by inversion of matrix $[Z(\omega)]$ at any required frequency. Obtaining the solution for tool dynamics, one may express the tool tip frequency response function which is necessary in constructing the stability lobes as

$$G_T(\omega) = C_1 e^{i\lambda L} + C_2 e^{-i\lambda L} + C_3 e^{\lambda L} + C_4 e^{-\lambda L},$$

$$\lambda^4 = \frac{m_2 \omega^2}{EI_2}. \quad (23)$$

The obtained model predicts the machining dynamics in different tool configurations. The mobility measurements are performed once to obtain the support flexibility functions $G_{ij}(\omega)$, $i, j = 1, 2$, and to identify the joint interface stiffness $K(x)$ and as long as the support dynamic flexibility functions and the joint interface stiffness remain constant the model is capable of predicting the machining dynamics at different tool configurations. Any change in tool configurations such as the change in its length, its diameter, etc. can be implemented in the model. In the developed method, the support dynamic flexibility matrix $[G(\omega)]$ and the stiffness and damping properties of elastic layer $K(x)$ are used as input information to predict the tool dynamics. The following provides an example on how the measurements are performed to obtain matrix $G(\omega)$ and the complex stiffness $K(x)$.

3. Experimental model identifications

Experimental setup used to obtain the support dynamic flexibility matrix $[G(\omega)]$ and also to identify the stiffness and damping properties of elastic layer $K(x)$ is shown in Fig. 2. In order to measure the support dynamic flexibility of a vertical three axis milling machine, two measurement points are selected on the holder. Fig. 3 and the direct and cross-mobility response functions are measured. The system is excited using an instrumented hammer (B&K8202) and the responses are measured using a uni-axial piezoelectric accelerometer (B&K4393). The time domain measurements are collected and transformed into frequency domain via a dual channel signal analyzer

(B&K2032). The measured receptance curves are shown in Fig. 4.

The coefficients of the joint interface polynomial are identified by conducting a separate set of experiments on the tool/holder/spindle assembly. In this experiment an extra long HSS DIN 1889/1 end mill with geometric properties, tabulated in Table 1, is mounted using a collet-type holder. An effective diameter for the fluted portion is

used in modelling following Schmitz's proposal [24], assuming that the equivalent cylindrical section in the model and the actual fluted portion have the same mass; the equivalent cylindrical section's diameter is considered to be 13.4 mm. A low-mass accelerometer is attached to the tool tip as shown in Fig. 2 and direct mobility measurements are performed using an impact test. The tool tip measured frequency response is employed in identifying the joint interface parameters, i.e. polynomial coefficients of the elastic joint interface layer.

The identification procedure in obtaining the elastic joint interface layer is based on minimizing the difference between the observed frequency response and the predictions of the model developed in Section 2. In this study, the joint interface model is identified in two steps: first a zero order model is adopted to approximate the joint interface stiffness function, next the order of function is increased to achieve improved correlation with the observed behavior of the machine tool.

3.1. Homogenous joint interface model

Initially, the joint interface stiffness is assumed to be homogenous. This corresponds to a $K(x)$ defined using a zero order polynomial function. Identification of such a function is straightforward and the obtained function can be used as a starting point in identifying the stiffness functions with higher order polynomial coefficients.

Using the measured frequency response curves of the support, shown in Fig. 3, and an initial estimate of the joint stiffness parameter the direct mobility at the tool tip is calculated. The tool tip frequency response is obtained using the procedure defined in Section 2 and the order of polynomial representing the inserted shank deformation is selected to be 15. The selection of the order is based on the fact that increasing it to a higher value does not have any effect on the tool response.

Next an objective function is formed comparing the difference between measured $G_m(\omega)$ and the estimated



Fig. 2. The test setup.

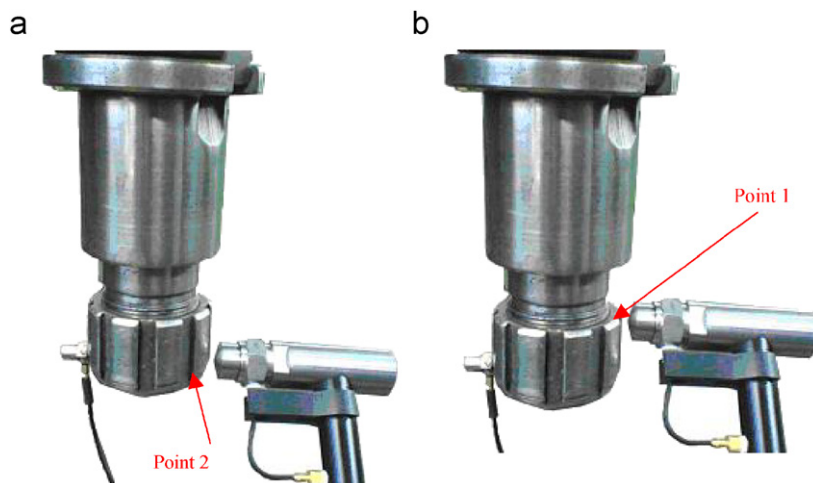


Fig. 3. Support frequency response measurements, direct (a) and cross (b).

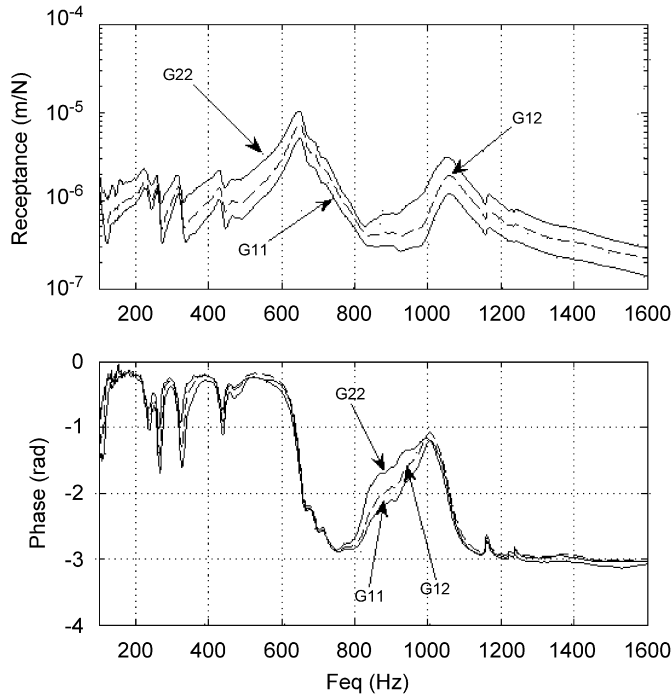


Fig. 4. Measured frequency response curves on the support points.

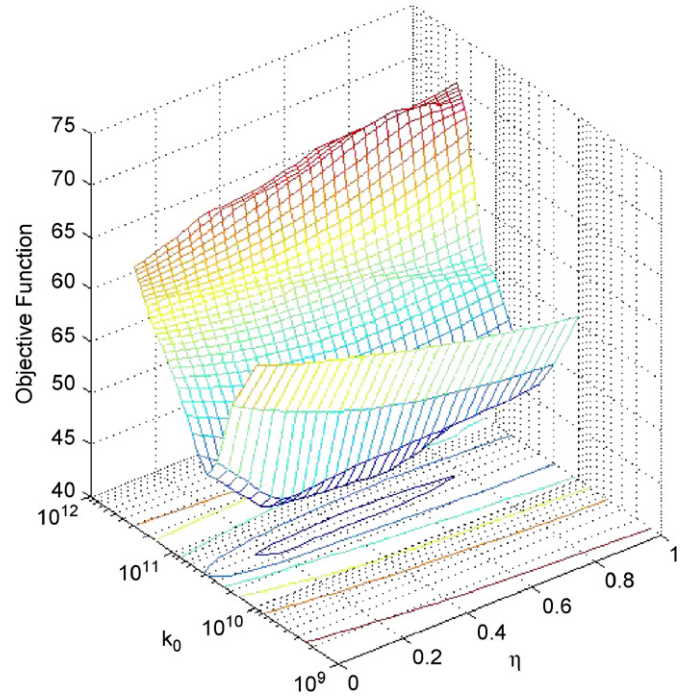


Fig. 5. 3-D plot of the objective function.

Table 1
Geometry of the tool (mm)

Total length	230
Shank length	40
Fluted diameter	18
Shank diameter	16

$G_c(\omega)$ tool tip frequency responses:

$$\min_{K_0} \| \log |G_m(\omega) - G_c(\omega)| \|_2 \quad (24)$$

The estimate for the joint stiffness parameter is adjusted in such a way that maximum agreement between measured and calculated frequency response curves is obtained and the objective function is minimized.

A 3-D plot of the objective function versus real and imaginary parts of the K_0 , i.e. stiffness and damping coefficient of the joint interface layer, is shown in Fig. 5. As shown in this figure the error is minimized when the contact parameters in the joint interface are set as $k = 3.5 \times 10^{10} \text{ N/m}^2$, $\eta = 0.4$. The calculated tool tip frequency response curves using the optimum parameters and corresponding measured values are compared in Fig. 6. These parameters provide a starting point in optimization procedures used in obtaining the higher order stiffness distribution polynomial coefficients.

3.2. First order joint interface model

Next a first order polynomial form is selected for the joint interface stiffness function $K(x)$. The parameters of

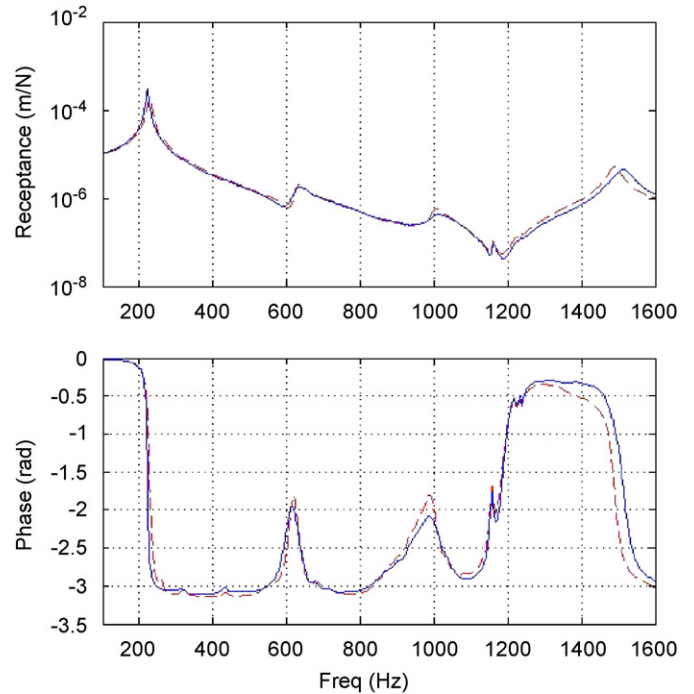


Fig. 6. The receptance curves at the tool tip, homogenous joint interface model (solid line), measurements (dashed line).

first order joint interface model are obtained by minimizing the objective function defined in Eq. (24). A nonlinear least square algorithm is used to minimize the objective function by tuning the parameters of joint interface. The zero order polynomial coefficients obtained in the previous section are employed as starting point in the optimization algorithm. The polynomial coefficients that minimize the objective

Table 2
The identified first order polynomial coefficients

K_0 (N/m ²)	K_1 (N/m ³)
$6.9(1 + 0.35i) \times 10^{10}$	$-8.25(1 + 0.35i) \times 10^{11}$

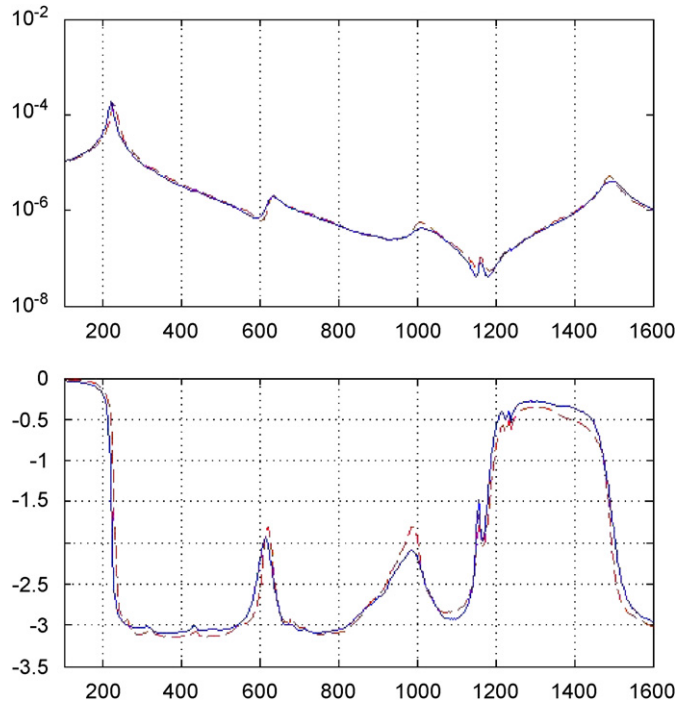


Fig. 7. The receptance curves at the tool tip, linearly varying joint interface model (solid line), measurements (dashed line).

function are tabulated in Table 2. The identified stiffness function shows a decreasing trend in contact stiffness between the tool and holder as x varies from zero to L_1 which is consistent with our expectation of behavior of such a joint. Increasing the order of polynomial from zero to one produces 7% decrease in the minimum value of the objective function in previous section which indicates further improvement of the model.

Using the obtained first order joint interface stiffness function the tool tip frequency response is calculated and is compared with the measured function in Fig. 7. An improvement in the model predictions especially in the vicinity of tool second mode at 1492 Hz is considerable. This demonstrates the efficiency of the proposed model in prediction of tool dynamics.

4. Results and discussions

An accurate model for prediction of tool dynamics is developed in previous sections. In the present section the performance of the model is investigated considering the tool dynamics in milling operation of an aluminum work piece. A step-by-step procedure to construct the tool tip

frequency response required for generating the stability lobes is as follows:

1. Development of an analytic model for tool similar to the one presented in Section 2.
2. Measuring the direct and cross-frequency response functions $G_{ij}(\omega)$, $i, j = 1, 2$, at points 1 and 2 on the holder, shown in Fig. 3, within frequency range of interest.
3. Identifying the elastic joint interface layer between tool and holder using procedures explained in Sections 3.1 and 3.2.
4. Incorporating the above information into Eqs. (17)–(21) to form matrix $[Z(\omega)]$ and to determine the unknown C_i , $i = 1, \dots, 4$.
5. Obtaining the tool tip frequency response from Eq. (23).
6. Evaluating the dynamics of the machining process using the obtained tool tip frequency response.

The stability diagrams are generated using the procedure presented by Budak and Altintas [2,3]. The required frequency responses for this procedure are generated using the developed model in Section 3.2. The obtained stability lobes are shown in Fig. 8. Next a tool tuning practice is performed using the developed model; the tool overhung length is varied and its dynamic is investigated at different configurations. The change in critical depth of cut, i.e. the stable depth of cut in a range of cutting speeds, is studied in terms of tool overhung length. The stability decreasing trend by increasing the tool length is observed in this practice, as shown in Fig. 9. Also the local increasing in stability diagram can be recognized in the figure in two specific tool overhung lengths i.e. 130 and 159 mm. At these two specific lengths the fundamental modes of

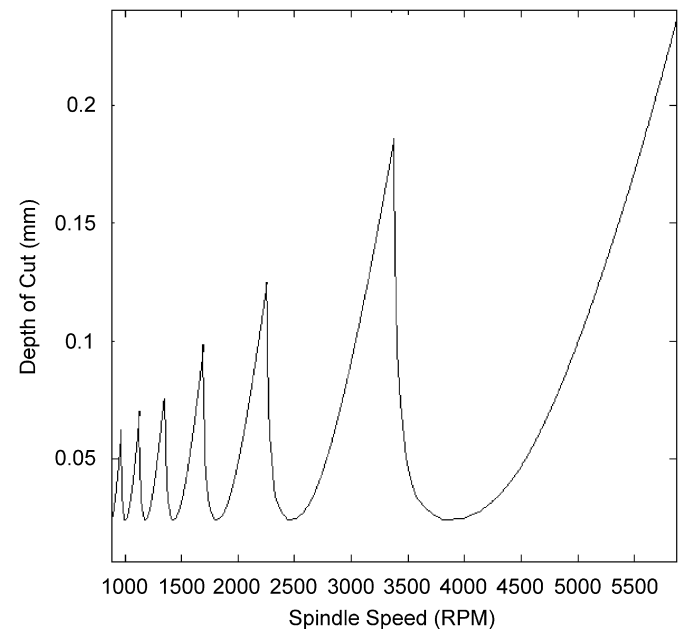


Fig. 8. The stability lobe diagram (tool overhung length 0.19 m).

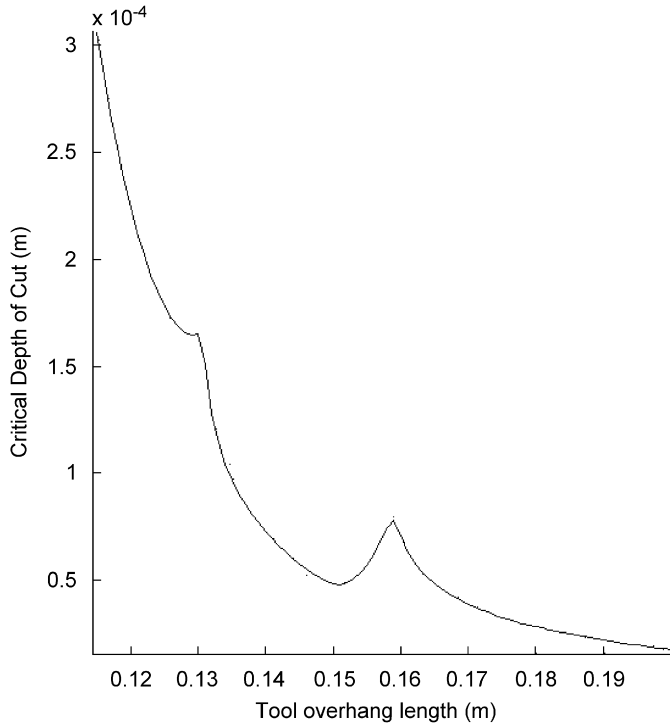


Fig. 9. Critical depth of cut versus overhung tool length.

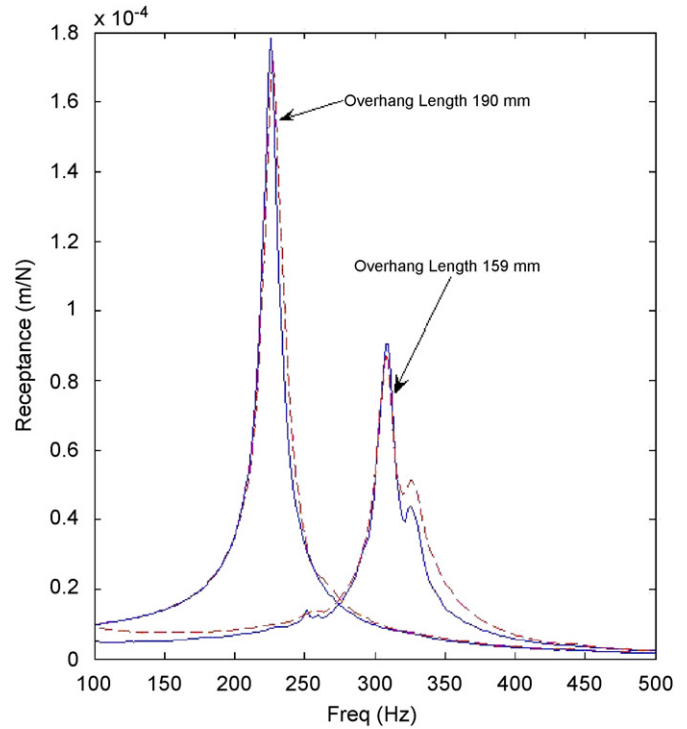


Fig. 11. Measured (dashed) and predicted (solid) receptance curves near the first mode.

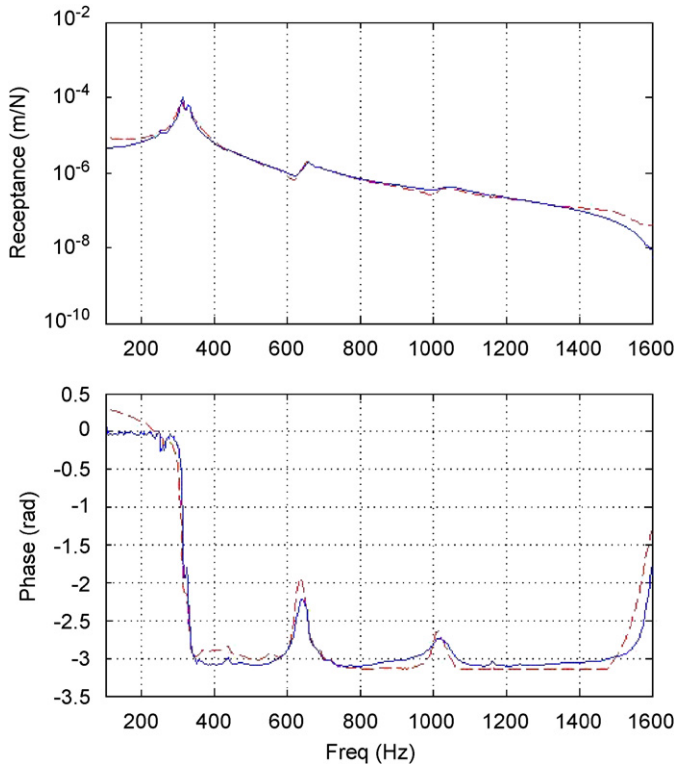


Fig. 10. Measured (dashed line) and predicted (solid line) receptance curves; overhung length 0.159 m.

tool overhung part are 428 and 314 Hz, respectively. The local increases in stability are justified considering the dynamic absorber effect of spindle modes on tool

vibration [12,13]; when the tool dominant mode corresponds with one of spindle natural frequencies, stability of the system increases. By inspecting the frequency responses of the holder–spindle assembly shown in Fig. 3 one can detect the resonances at 314 and 428 Hz. There are two specific tool lengths within range of interest in which the tool dominant mode of vibration and one of the spindle modes match; the tool length can be tuned so that the dynamic vibration absorbing phenomenon comes into effect, hence obtaining the optimum tool overhung length.

To validate the predictions of the model, the tool length is changed to 159 mm and frequency response function is measured at the tool tip. Predicted and measured frequency response curves are shown in Fig. 10; there is an excellent agreement between the two responses indicating the accuracy of presented model in prediction of tool dynamics in different configurations. Fig. 11 compares the tool tip frequency responses at two different tool lengths: 190 and 159 mm; by decreasing the tool length the first mode of spindle at 314 Hz interacts with the first mode of tool overhung length and produces a double peak in the frequency response plot at this frequency due to dynamic vibration absorption effect.

This experimental case study reflects the fact that the developed model is capable of accurately predicting the milling dynamics, including the dynamic vibration absorber effect due to spindle modes of vibrations, demonstrated by a tool tuning practice.

5. Conclusions

A new approach in modelling high-speed machining dynamics is presented using the measured dynamic flexibility of the holder–spindle assembly and an analytic model for the tool. This enables the analyst to model the machining dynamics in various tool combinations without the need for repeated measurements. The joint between the tool and holder unlike other commonly used models which employ lumped stiffness and viscous dashpots is represented using a zero thickness distributed interface layer with variable stiffness. The proposed tool–holder distributed parameter joint interface takes into account the change in normal stiffness along the tool shank part. This variation is due to the change in normal pressure along the joint interface. The model also uses a displacement-dependent damping mechanism to account for structurally damped characteristics of the interface. The interface layer parameters are identified using experimentally observed behavior of the tool–holder–spindle assembly.

An experimental study is performed to verify the effectiveness of the proposed model and its capability in

predicting the structure dynamics. A physically justifiable linearly varying tool–holder interface stiffness function is identified from the measured results and the tool dynamics is predicted using the proposed model. The linear variation of the interface stiffness is due to the mechanism used to join the tool and holder. Employing such an interface layer in modelling significantly improves predictions of machining dynamics. It is shown using an experimental case study that the developed model is capable of accurately predicting the milling dynamics, including the dynamic vibration absorber effect due to spindle modes of vibrations, demonstrated by a tool tuning practice.

The accuracy of model in predicting the frequency responses of the machine at various tool configurations and its ability to demonstrate the physical phenomena involved in the machine structure such as dynamic vibration absorbing effect are demonstrated in the case studies. The results reflect the fact that the assumptions made in constructing the model are based on valid engineering judgments and the model can be used to predict the machine dynamics at working conditions beyond those considered in this study.

Appendix A

In this Appendix the entries of matrices $[T_v]$, $[T_a]$, $[R]$ and $[Z]$ are derived.

Based on the recursive equations (16) the entries of matrices $[T_v]$, $[T_a]$ when the interface stiffness function $K(x)$ is assumed to be linear take the following forms:

$$[T_a] = \frac{1}{EI_1} \begin{bmatrix} 1 & 0 & 0 & 0 \\ 0 & 1 & 0 & 0 \\ 0 & 0 & 1 & 0 \\ 0 & 0 & 0 & 1 \\ \frac{m_1\omega^2 - K_0}{24} & 0 & 0 & 0 \\ \frac{-K_1}{120} & \frac{m_1\omega^2 - K_0}{120} & 0 & 0 \\ 0 & \frac{-K_1}{720} & \frac{m_1\omega^2 - K_0}{720} & 0 \\ 0 & 0 & \frac{-K_1}{7 \times 720} & \frac{m_1\omega^2 - K_0}{7 \times 720} \\ \frac{m_1\omega^2 - K_0}{8 \times 7 \times 720} \left(\frac{m_1\omega^2 - K_0}{24} \right) & 0 & 0 & \frac{-K_1}{8 \times 7 \times 720} \\ \cdot & \cdot & \cdot & \cdot \\ \cdot & \cdot & \cdot & \cdot \\ \cdot & \cdot & \cdot & \cdot \end{bmatrix} \quad (A.1)$$

The first few rows of matrix $[T_a]$ are derived and the rest can be obtained from Eq. (16). In case of matrix $[T_v]$ entries of the rows 5–7 are non-zero and the rest are zeros:

$$[T_v] = \frac{1}{EI_1} \begin{bmatrix} 0 & 0 \\ 0 & 0 \\ 0 & 0 \\ 0 & 0 \\ \frac{K_0 L_1}{24d} & \frac{K_0(1 - L_1/d)}{24} \\ \frac{(K_1 L_1/d - K_0/d)}{120} & \frac{(K_0/d + K_1(1 - L_1/d))}{120} \\ -\frac{K_1}{720d} & \frac{K_1}{720d} \\ 0 & 0 \\ \cdot & \cdot \\ \cdot & \cdot \\ \cdot & \cdot \end{bmatrix}. \tag{A.2}$$

Entries of matrix $[R]$, used in Eqs. (18) and (19), are obtained by introducing the inserted shank deflection shape, Eq. (14), into the right-hand side of Eq. (11):

$$\begin{aligned} & \left\{ \begin{array}{l} K \int_0^{L_1} K(x) \frac{L_1 - x}{d} \Phi(x) dx \\ \int_0^{L_1} K(x) \left(1 - \frac{L_1 - x}{d} \right) \Phi(x) dx \end{array} \right\} \\ &= \left\{ \begin{array}{l} \int_0^{L_1} \frac{L_1 K(x)}{d} \sum_{n=1}^N a_n x^{n-1} dx - \int_0^{L_1} \frac{K(x)}{d} \sum_{n=1}^N a_n x^n dx \\ \int_0^{L_1} K(x) \sum_{n=1}^N a_n x^{n-1} dx - \int_0^{L_1} \frac{K(x)L_1}{d} \sum_{n=1}^N a_n x^{n-1} dx + \int_0^{L_1} \frac{K(x)}{d} \sum_{n=1}^N a_n x^n dx \end{array} \right\} \\ &= \left[\begin{array}{ll} \int_0^{L_1} \left(\frac{L_1 K(x)}{d} - \frac{K(x)x}{d} \right) dx & \int_0^{L_1} \left(\frac{L_1 K(x)x}{d} - \frac{K(x)x^2}{d} \right) dx \quad \dots \\ \int_0^{L_1} \left(\frac{K(x)}{1} - \frac{K(x)L_1}{d} + \frac{K(x)x}{d} \right) dx & \int_0^{L_1} \left(\frac{K(x)x}{1} - \frac{K(x)L_1 x}{d} + \frac{K(x)x^2}{d} \right) dx \quad \dots \end{array} \right] \\ & \dots \left[\begin{array}{l} \int_0^{L_1} \left(\frac{L_1 K(x)x^{N-1}}{d} - \frac{K(x)x^N}{d} \right) dx \\ \int_0^{L_1} \left(\frac{K(x)x^{N-1}}{1} - \frac{K(x)L_1 x^{N-1}}{d} + \frac{K(x)x^N}{d} \right) dx \end{array} \right] \left\{ \begin{array}{l} a_1 \\ \vdots \\ a_N \end{array} \right\} = [R] \left\{ \begin{array}{l} a_1 \\ \vdots \\ a_N \end{array} \right\}. \tag{A.3}$$

The matrix $[Z]$ introduced in Eq. (22) has the following form:

$$\begin{bmatrix}
 EI_2 i \lambda^3 e^{i\lambda L} & -EI_2 i \lambda^3 e^{-i\lambda L} & -EI_2 \lambda^3 e^{L\lambda} & EI_2 \lambda^3 e^{-\lambda L} & 0 & 0 & 0 & 0 & 0 & 0 \\
 -\lambda^2 e^{i\lambda L} & -\lambda^2 e^{-i\lambda L} & \lambda^2 e^{L\lambda} & \lambda^2 e^{-\lambda L} & 0 & 0 & 0 & 0 & 0 & 0 \\
 0 & 0 & 0 & 0 & 2S_{31} & 0 & 0 & 0 & 0 & 0 \\
 0 & 0 & 0 & 0 & 6S_{41} & 0 & 0 & 0 & 0 & 0 \\
 -e^{i\lambda L_1} & -e^{-i\lambda L_1} & -e^{\lambda L_1} & -e^{-\lambda L_1} & \sum_{j=1}^N L_1^{j-1} S_{j1} & 0 & 0 & 0 & 0 & 0 \\
 -i\lambda e^{i\lambda L_1} & i\lambda e^{-i\lambda L_1} & -\lambda e^{\lambda L_1} & \lambda e^{-\lambda L_1} & \sum_{j=2}^N (j-1)L_1^{j-2} S_{j1} & 0 & 0 & 0 & 0 & 0 \\
 EI_2 \lambda^2 e^{i\lambda L_1} & EI_2 \lambda^2 e^{-i\lambda L_1} & -EI_2 \lambda^2 e^{\lambda L_1} & -EI_2 \lambda^2 e^{-\lambda L_1} & EI_1 \sum_{j=3}^N (j-1)(j-2)L_1^{j-3} S_{j1} & 0 & 0 & 0 & 0 & 0 \\
 EI_1 i \lambda^3 e^{i\lambda L_1} & -EI_1 i \lambda^3 e^{-i\lambda L_1} & -EI_1 \lambda^3 e^{\lambda L_1} & EI_1 \lambda^3 e^{-\lambda L_1} & EI_1 \sum_{j=4}^N (j-1)(j-2)(j-3)L_1^{j-4} S_{j1} & 0 & 0 & 0 & 0 & 0 \\
 0 & 0 & 0 & 0 & 0 & 0 & 0 & 0 & 0 & 0 \\
 0 & 0 & 0 & 0 & 0 & 0 & 0 & 0 & 0 & 0 \\
 2S_{32} & 0 & 2S_{33} & 0 & 2S_{34} & 0 & 0 & 0 & 0 & 0 \\
 6S_{42} & 0 & 6S_{43} & 0 & 6S_{44} & 0 & 0 & 0 & 0 & 0 \\
 \sum_{j=1}^N L_1^{j-1} S_{j2} & 0 & \sum_{j=1}^N L_1^{j-1} S_{j3} & 0 & \sum_{j=1}^N L_1^{j-1} S_{j4} & 0 & 0 & 0 & 0 & 0 \\
 \sum_{j=2}^N (j-1)L_1^{j-2} S_{j2} & 0 & \sum_{j=2}^N (j-1)L_1^{j-2} S_{j3} & 0 & \sum_{j=2}^N (j-1)L_1^{j-2} S_{j4} & 0 & 0 & 0 & 0 & 0 \\
 EI_1 \sum_{j=3}^N (j-1)(j-2)L_1^{j-3} S_{j2} & 0 & EI_1 \sum_{j=3}^N (j-1)(j-2)L_1^{j-3} S_{j3} & 0 & EI_1 \sum_{j=3}^N (j-1)(j-2)L_1^{j-3} S_{j4} & 0 & 0 & 0 & 0 & 0 \\
 EI_1 \sum_{j=4}^N (j-1)(j-2)(j-3)L_1^{j-4} S_{j2} & 0 & EI_1 \sum_{j=4}^N (j-1)(j-2)(j-3)L_1^{j-4} S_{j3} & 0 & EI_1 \sum_{j=4}^N (j-1)(j-2)(j-3)L_1^{j-4} S_{j4} & 0 & 0 & 0 & 0 & 0
 \end{bmatrix}, \tag{A.4}$$

where S_{ij} are entries of matrix $[S]$ defined in Eq. (19).

References

[1] S.A. Tobias, Machine Tool Vibration, Blackie, London, 1965.
 [2] E. Budak, Y. Altintas, Analytical prediction of chatter stability in milling—part I: general formulation, Transactions of the ASME, Journal of Dynamic Systems, Measurement, and Control 120 (1998) 22–30.
 [3] E. Budak, Y. Altintas, Analytical prediction of chatter stability in milling—part II: application of general formulation to common milling systems, Transactions of the ASME, Journal of Dynamic Systems, Measurement, and Control 120 (1998) 31–36.
 [4] J. Tlustý, Dynamics of high-speed milling, Transactions of the ASME Journal of Engineering for Industry 108 (1986) 59–67.
 [5] N.H. Hanna, S.A. Tobias, A theory of nonlinear regenerative chatter, Transactions of the ASME Journal of Engineering for Industry (1974) 247–255.
 [6] H.E. Merritt, Theory of self-excited machine-tool chatter, Transactions of the ASME Journal of Engineering for Industry (1965) 447–454.
 [7] R. Sridhar, R.E. Hohn, G.W. Long, A general formulation of milling process equation, Transactions of the ASME Journal of Engineering for Industry (1968) 317–324.
 [8] E.B. Kivanc, E. Budak, Structural modeling of end mills for form error and stability analysis, International Journal of Machine Tools and Manufacture 44 (11) (2004) 1151–1161.
 [9] E. Budak, Analytical models for high performance milling. Part I: cutting forces, structural deformations and tolerance integrity, International Journal of Machine Tools and Manufacture 46 (12–13) (2006) 1478–1488.
 [10] E. Budak, Analytical models for high performance milling. Part II: process dynamics and stability, International Journal of Machine Tools and Manufacture 46 (12–13) (2006) 1478–1488.
 [11] H. Ahmadian, M. Salahshour, Predicting chatter in milling using a beam model on elastic support, in: Proceedings of the Tehran International Congress on Manufacturing Engineering, Tehran, Iran, December 12–15, 2005.
 [12] T.L. Schmitz, Predicting high-speed machining dynamics by substructure analysis, Annals of the CIRP (2000) 303–308.

- [13] T.L. Schmitz, M.A. Davies, M.D. Kennedy, Tool point frequency response prediction for high-speed machining by RCSA, Transactions of the ASME, Journal of Manufacturing Science and Engineering 123 (2001) 700–707.
- [14] S.S. Park, Y. Altintas, M. Movahhedy, Receptance coupling for end mills, International Journal of Machine Tools and Manufacture 43 (2003) 889–896.
- [15] M.R. Movahhedy, J.M. Gerami, Prediction of spindle dynamics in milling by sub-structure coupling, International Journal of Machine Tools and Manufacture 46 (2006) 243–251.
- [16] G.S. Duncan, M.F. Tummond, T.L. Schmitz, An investigation of the dynamic absorber effect in high-speed machining, International Journal of Machine Tools and Manufacture 45 (2005) 497–507.
- [17] T.L. Schmitz, G.S. Duncan, Receptance coupling for dynamic prediction of assemblies with coincident neutral axes, Journal of Sound and Vibration 289 (2006) 1045–1065.
- [18] T.L. Schmitz, K. Powell, D. Won, G.S. Duncan, W.G. Sawyer, J.C. Ziegert, Shrink fit tool holder connection stiffness/damping modeling for frequency response prediction in milling, part 1: receptance model, in: Proceedings of the second CIRP-HPC 2006, Vancouver, Canada, 2006.
- [19] T.L. Schmitz, K. Powell, D. Won, G.S. Duncan, W.G. Sawyer, J.C. Ziegert, Shrink fit tool holder connection stiffness/damping modeling for frequency response prediction in milling, part 2: finite element model, in: Proceedings of the second CIRP-HPC 2006, Vancouver, Canada, 2006.
- [20] A. Erturk, H.N. Ozguven, E. Budak, Effect analysis of bearing and interface dynamics on tool point FRF for chatter stability in machine tools by using a new analytical model for spindle–tool assemblies, International Journal of Machine Tools and Manufacture 47 (2007) 23–32.
- [21] A. Erturk, H.N. Ozguven, E. Budak, Analytical modelling of spindle–tool dynamics on machine tools using Timoshenko beam model and receptance coupling for the prediction of tool point FRF, International Journal of Machine Tools and Manufacture 46 (2006) 1901–1912.
- [22] I.M. Hanna, J.S. Agapiou, D.A. Stephenson, Modeling the HSK toolholder–spindle interface, Transactions of the ASME, Journal of Manufacturing Science and Engineering 124 (2002) 734–744.
- [23] M. Eisenberger, Vibration frequencies for beams on variable one- and two-parameter elastic foundations, Journal of Sound and Vibration 176 (5) (1994) 577–584.
- [24] T.L. Schmitz, T.J. Burns, J.C. Ziegert, B. Dutterer, W.R. Winfough, Tool length-dependent stability surfaces, Machining Science and Technology 8 (3) (2004) 377–397.